# Observation of Many-Body Quantum Phase Transitions beyond the Kibble-Zurek Mechanism

Qi Huang,[1] Ruixiao Yao,[2,*] Libo Liang,[1] Shuai Wang,[2] Qinpei Zheng,[1] Dingping Li,[3] Wei Xiong,[1] Xiaoji Zhou,[1] Wenlan Chen,[2,4,†] Xuzong Chen,[1,‡] and Jiazhong Hu[2,4,§]

[1]*School of Electronics Engineering and Computer Science, Peking University, Beijing 100871, China*
[2]*Department of Physics and State Key Laboratory of Low Dimensional Quantum Physics, Tsinghua University, Beijing 100084, China*
[3]*School of Physics, Peking University, Beijing 100871, China*
[4]*Frontier Science Center for Quantum Information, Beijing 100084, China*

(Received 26 December 2020; revised 23 August 2021; accepted 8 October 2021; published 11 November 2021)

Quantum critical behavior of many-body phase transitions is one of the most fascinating yet challenging questions in quantum physics. Here, we improved the band-mapping method to investigate the quantum phase transition from superfluid to Mott insulators, and we observed the critical behaviors of quantum phase transitions in both the dynamical steady-state-relaxation region and the phase-oscillation region. Based on various observables, two different values for the same quantum critical parameter are observed. This result is beyond a universal-scaling-law description of quantum phase transitions known as the Kibble-Zurek mechanism, and suggests that multiple quantum critical mechanisms are competing in many-body quantum phase transition experiments in inhomogeneous systems.

DOI: 10.1103/PhysRevLett.127.200601

Nonequilibrium quantum physics is one of the most challenging topics in quantum physics, related with many different areas such as quantum matters [1,2], many-body correlations [3,4], and quantum simulations [5–9]. One central question among the nonequilibrium quantum physics is how to understand quantum critical behaviors and dynamics of the quantum phase transitions (QPT). The Kibble-Zurek mechanism (KZM) [10,11] originating from thermodynamics [12–16], describes dynamics of QPT with symmetry breaking [17–22], where the order parameter can be well defined and the quantum critical behaviors have a universal scaling-law dependence on the external ramping speed. As for the development of QPT, the energy gap as well as the symmetry breaking becomes one of the critical conditions of phase transitions. Thus, it becomes interesting to investigate many-body quantum phase transitions entering symmetry-conserved phases with open energy gaps, which is on the opposite side of the conventional KZM.

The superfluid (SF) to Mott insulators (MI) phase transition is one of the most important QPT in many-body physics. Seminal experiments [23,24] explored the KZM based on transitions from symmetry-conserved MI to symmetry-broken SF with gap closing, where the measured quantum critical parameters are not consistent with the theoretical predictions [25,26]. Here, we investigate the many-body QPT, where the system transits from the SF phase (gapless symmetry broken) to the MI phase (gapped symmetry conserved) with an improved band-mapping method. In such gap-opening QPT, the quantum criticality is described by the energy gap $\Delta$ versus the distance $g$ to quantum critical point in phase diagrams with a scaling law $\Delta \propto |g|^{\nu z}$, where $\nu z$ is a quantum critical parameter. The value of $\nu z$ decides the spatial-temporal universal dynamics in KZM [18,27–32]. Based on various observables, we extract out two different values for the same critical parameter $\nu z$. Both values were predicted theoretically [25,26], but the coexistence of two different values for the same parameter violates the universality of KZM. Besides, we observe dynamical steady-phase relaxations within the KZM frame transiting into non-steady-phase oscillations which is beyond the KZM frame. In fact, the open gap in the many-body systems allows different values of critical parameters to exist in the same QPT, protects phase oscillations and thus boosts the many-body QPT beyond the conventional symmetry-breaking KZM.

Our experiment is performed in a three-dimensional optical lattice formed by three standing waves perpendicular to each other at wavelength $\lambda = 1064$ nm [Fig. 1(a)], and the magnetic field is applied along the $z$ axis. We prepare Bose-Einstein condensates of $^{87}$Rb atoms in $|F = 1, m_F = -1\rangle$ and then load them into 3D homogeneous lattices with trap depth $V = 5E_r$ and atom number $N = 1.1(2) \times 10^5$ [33–35]. Here, $V$ is the trap depth generated by one lattice beam and $E_r = h \times 2$ kHz is the recoil energy of lattice beams. Because of the Gaussian shape of lattice beams, the lattices are printed by an external harmonic trap with homogeneous radial vibrational frequencies $\sim 2\pi \times 20(1)$ Hz. The system is described by a Bose-Hubbard model in an external harmonic trap [25,36]:

 

$$H = -J\sum_{\langle i,j\rangle}(\hat{a}_i^\dagger \hat{a}_j + \text{H.c.}) + \frac{1}{2}U\sum_i \hat{n}_i(\hat{n}_i - 1) + \sum_i\left(\frac{1}{2}m\omega_0^2 r_i^2 - \mu\right)\hat{n}_i, \quad (1)$$

where $a_i$ (or $a_i^\dagger$) is the annihilation (or creation) operator of a boson at the lattice site $i$, $J$ is the tunneling coefficient, $U$ is the on-site interaction, $\mu$ is the chemical potential, and $\frac{1}{2}m\omega_0^2 r_i^2$ describes the external harmonic trap. Since the atomic cloud size is much smaller than the waist of lattice beams, the inhomogeneity of $J$ and $U$ are negligible in this model [see Supplemental Material (SM) [37], section I, SM-I].

Comparing with the previous band-mapping method [38] requiring adiabatically turning off three lattice beams, here we instantaneously turn off the $z$ lattice that is along the imaging direction [Fig. 1(a)]. The atomic gas expands along $z$ quickly, releases the interaction energy, and the momentum distribution along $z$ does not contribute to the band-mapping image. It helps to avoid the fast relaxations in the $x$-$y$ plane in the subsequent expansion. At the same time when the $z$ lattice is turned off, we ramp down the $x$ and $y$ lattices in 2 ms, which is slow enough to adiabatically convert the quasimomentum into the real momentum. Then the time of flight is applied to measure the momentum distribution in the $x$-$y$ plane. Using this technique, we are able to obtain better quasimomentum distributions of atoms in the interacting system [Fig. 1(b) and SM-II [37] ], where the incoherent atoms in the first Brillouin zone are exactly mapped to a square shape and displays a flat plateau, while the phase coherent superfluid component corresponds to a narrow and sharp peak at the zero-momentum point. This helps us to quantify the coherence across the whole system [Fig. 1(b)] and to observe the dynamical response at different ramping rates [Figs. 1(c) and 1(d)]. We define the incoherent fraction $\gamma_{\text{inc}}$, as the ratio of the integrated optical depth of the flat plateau divided by the total integrated optical depth [Fig. 1(b) and SM-III [37] ] based on the band-mapping images.

To study the dynamics of QPT, we first prepare the superfluid at $V_0 = 5E_r$ and hold it for 20 ms. Then, we ramp up the trap depth $V$ linearly with a ramping rate $k$ [Fig. 2(a)]. For each $k$, we perform the band mapping at different $V$ and measure the corresponding incoherent fraction $\gamma_{\text{inc}}$ [Fig. 2(b)]. According to Refs. [36,39], the MI starts to appear at $V_c = 13E_r$ for $^{87}$Rb in 3D optical lattices. We find two different response regions before and after ramping through $V_c$. In the SF region, the system responses to the ramping rapidly due to its gapless nature. We measure the response time $\tau_{\text{SF}}$ by defining the time to reach $\gamma_{\text{inc}} = 0.6$ and obtain a scaling-law dependence $\tau_{\text{SF}} \propto k^{-0.91(3)}$, slightly delayed from the ideal instant response $k^{-1}$. We performed numerical calculations by the Gutzwiller mean field theory (GMFT) [40,41], finding it consistent with the experimental results [Fig. 2(c)]. However, once the trap depth is above $V_c$, $\gamma_{\text{inc}}$ starts to furcate and show retarded or oscillating responses depending on $k$.

For a slow ramp ($k \leq 4E_r/\text{ms}$), the response in the MI region is trying to approach the steady state with a dynamical relaxation time $\tau_{\text{MI}}$. In Fig. 2(d), we extract $\tau_{\text{MI}}$ based on the time duration to reach $\gamma_{\text{inc}} = 0.9$ from the time at trap depth $13E_r$ [18]. It shows a scaling-law

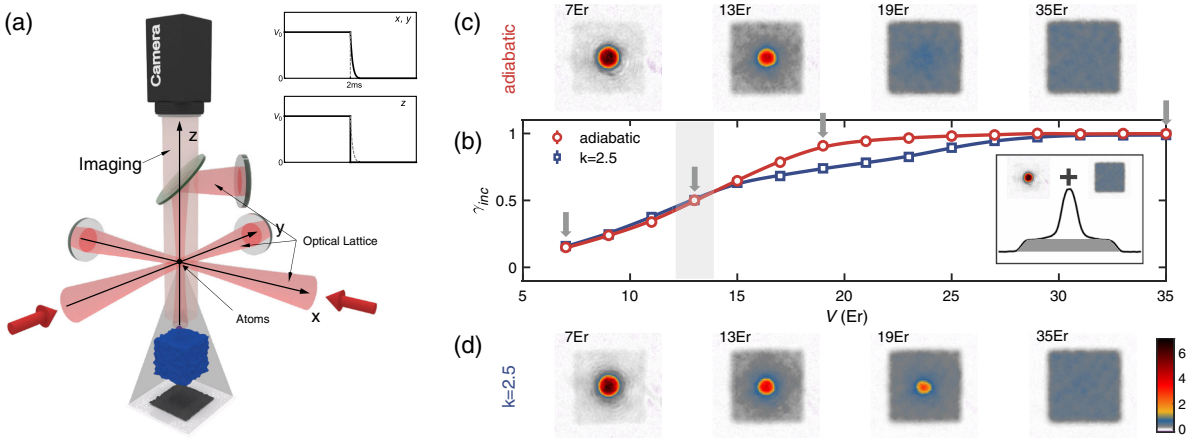


FIG. 1. Experimental setup and improved band-mapping method. (a) Three orthogonal standing waves form 3D optical lattices for $^{87}$Rb, and absorption images are taken along the $z$ direction. The inset: the $z$ lattice is turned off instantaneously while the $x$ and $y$ lattices are ramped down in 2 ms for the band mapping. (b) The incoherent fraction $\gamma_{\text{inc}}$ versus the trap depth $V$ for the SF-MI phase transitions. The red circles correspond to the measurement with adiabatic ramping, while the blue squares correspond to the measurement with linear ramping at rates $k = 2.5E_r/\text{ms}$. The shadow area locates quantum phase transition at $V_c = 13E_r$ for $\bar{n} = 1$'s lobe. Gray arrows indicate data in the panel (c) and (d). The inset shows the decomposition of quasimomentum profiles and analysis of $\gamma_{\text{inc}}$. (c) and (d) The band mapping profiles performed at trap depth $V = 7$, 13, 19, and $35E_r$. Error bars (1 standard deviation) are smaller than the marker size.

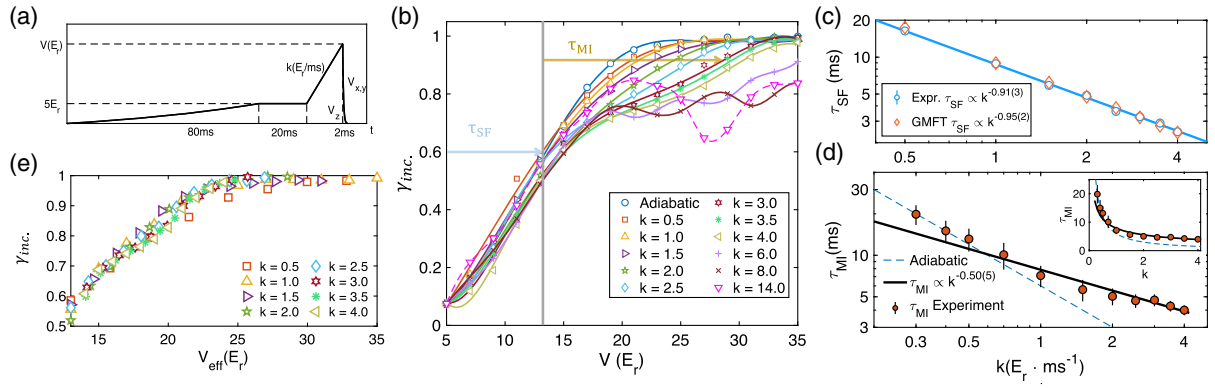


FIG. 2. Dynamical response of SF-MI phase transitions. (a) The time sequence of the trap depth ramping. The first stage of 80 ms and the second stage of 20 ms prepare superfluid samples from the condensates. The third stage is the linear ramp with a ramping rate $k$ when the atoms experience phase transitions. The final stage is the band mapping to distinguish the coherent component from the incoherent one. (b) The incoherent fraction $\gamma_{\mathrm{inc}}$ versus trap depth $V$ for different $k$. The scattered markers are the experimental data and the solid lines are the polynomial fits (see SM-V [37]). A furcation appears at critical point $V_c = 13E_r$. And $\gamma_{\mathrm{inc}}$ approaches 1 for different ramping rate $k$ for small $k$. When $k$ gets larger, $\gamma_{\mathrm{inc}}$ starts to oscillate with retard thermalization. The pink triangles denote the dynamics at $k = 14E_r/\mathrm{ms}$, which oscillates drastically and fail to relax. Here we label the definition of SF response time $\tau_{\mathrm{SF}}$ (time to reach $\gamma_{\mathrm{inc}} = 0.6$) and the MI dynamical relaxation time $\tau_{\mathrm{MI}}$ (time between $\gamma_{\mathrm{inc}} = 0.6$ and $\gamma_{\mathrm{inc}} = 0.9$) on the plot. (c) $\tau_{\mathrm{SF}}$ versus $k$. The blue circles are the experimental data and the blue solid line is the fit based on power laws with $\tau_{\mathrm{SF}} \sim k^{-0.91(3)}$. The red diamonds are the GMFT simulation with a fit $\tau_{\mathrm{SF}} \propto k^{-0.95(2)}$. (d) $\tau_{\mathrm{MI}}$ versus $k$. The red filled circles are the extracted data. The blue dashed line is $\tau_{\mathrm{MI}} \sim k^{-1}$ for the adiabatic response (see SM-VI [37]). The black solid line is the fit with $\tau_{\mathrm{MI}} \sim k^{-0.50(5)}$ for $k \geq 0.7E_r/\mathrm{ms}$, which indicates $\nu z = 1.0(2)$. (e) The universal response of $\gamma_{\mathrm{inc}}$ versus the rescaled trap depth $V_{\mathrm{eff}}$, where $V_{\mathrm{eff}} = (V - V_c)k^{-(1-0.50)} + V_c$ and $k$ is in the unit of $E_r/\mathrm{ms}$. Error bars (see SM-V [37]) correspond to 1 standard deviation.

dependence of nonadiabatic response $\tau_{\mathrm{MI}} \propto k^{-0.50(5)}$ for $k \geq 0.7E_r/\mathrm{ms}$. In Sec. VI of the Supplemental Material [37], we verify that the exponent near $-0.5$ is not sensitive to the end point $\gamma_{\mathrm{inc}}$ we choose. The KZM predicts the dependence of the freeze-out time $\tau$ on the ramping rate $k$ to be [18,27–29]

$$\tau \propto k^{-\frac{\nu z}{1+\nu z}}, \tag{2}$$

where $\tau$ characterizes the time of relaxation. Based on this form, we obtain the critical parameter $\nu z = 1.0(2)$ by measuring the MI dynamical relaxation time, and infer $\nu = 1/2$ and $z = 2$ corresponding to the off-tip critical parameters with linear gap opening in the SF-MI phase diagram [25]. To show the quantum criticality, we rescale the horizontal axis of Fig. 2(b) at $V_c$ to be $V_{\mathrm{eff}} = (V - V_c)k^{-(1-0.50)} + V_c$. The different sets of $\gamma_{\mathrm{inc}}$ data fall into one universal curve [Fig. 2(e)] in the MI region. This shows the universality of the KZM if we consider only $\tau_{\mathrm{MI}}$ under a slow ramp $k$. However, GMFT cannot describe this relaxations (see SM-VII [37]) due to strong interactions of deep MI [39].

Besides a scaled relaxation time, the KZM also predicts universally scaled defect density introduced by crossing the phase transition. Here we use the excitation fraction $n_{\mathrm{ex}}$ to characterize the defects, where it describes how many atoms are excited comparing to ground-state Mott insulators. $n_{\mathrm{ex}}$ follows the form of [27,30–32]:

$$n_{\mathrm{ex}} \propto k^{\frac{d\nu}{1+\nu z}}. \tag{3}$$

Here $d = 3$ is the dimension of 3D optical lattices. We analyze the excitation fraction as the components of MI fractions deviated from its adiabatic value [23]: $n_{\mathrm{ex}}(V,k) = \gamma_{\mathrm{inc}}(V,\mathrm{adia}) - \gamma_{\mathrm{inc}}(V,k)$. For $V > V_c$, this definition quantifies the additional particle-hole pairs on top of the MI ground state with quantum fluctuations, which retains additional phase coherence due to the nonequilibrium dynamics (see SM-VII [37] for more analysis). In Fig. 3(a), we plot $n_{\mathrm{ex}}(V,k)$ and obtain a scaling-law $n_{\mathrm{ex}} \propto k^{0.97(12)}$. The value of $n_{\mathrm{ex}}(V,k)$ depends on the chosen trap depth $V$, but the value of fitted-exponent $\alpha$ is robust against different $V$ [Fig. 3(b)]. The fitting on Eq. (3) shows $\nu z = 0.48(9)$, where we infer $\nu = 1/2$ and $z = 1$, corresponding to the on-tip critical parameters with square-root gap opening in the SF-MI phase diagram [25]. To better understand this result, we apply GMFT in the shallow MI region and find the defect density due to the nonequilibrium dynamics has a scaling factor of 0.97(5), consistent with our observations (see SM-VII [37]).

For a fast ramp ($k \geq 6E_r/\mathrm{ms}$), the system response enters a non-steady-state region where $\gamma_{\mathrm{inc}}$ oscillates with time. This provides a smooth connection from the adiabatically ramping to the fast ramping [42]. In this region, the multiple-atom occupancies in the SF are frozen rapidly without relaxations. However, the phase coherence between single and multiple occupancies does not disappear immediately and oscillates at the frequency of $U/\hbar$. To visualize the oscillation, we hold the lattice for a time interval $t$ after the ramping, where a larger $k$ leads to a

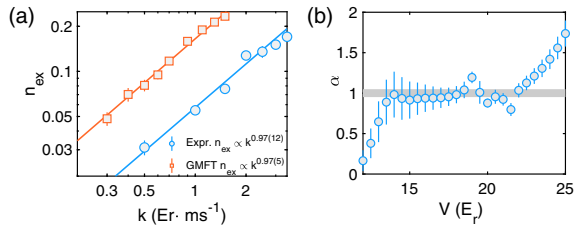


FIG. 3. Excitation fraction $n_{\mathrm{ex}}$ in the MI region. (a) $n_{\mathrm{ex}}(k)$ measured at $V \sim 18E_r$ (SM-VI [37]). Blue circles are experimental results with the blue line fit of $n_{\mathrm{ex}} \sim k^{\alpha}$ at $\alpha = 0.97(12)$. Orange squares are GMFT simulation results with the orange line fit of $n_{\mathrm{ex}} \sim k^{\alpha}$ at $\alpha = 0.97(5)$. (b) The fitted scaling coefficient $\alpha$ is robust against the chosen trap depth $V$, as long as $V > 13E_r$ (goes through phase transition) and $V < 19E_r$ (far from deep MI region). Error bars correspond to 1 standard deviation.

larger oscillation amplitude $A$ [Figs. 4(a) and 4(b)]. The fit shows $A \propto k^{1.49(17)}$ [Fig. 4(c)]. In GMFT we see similar trends, where $A \propto k^{1.41(15)}$ is obtained. Since we stop ramping at deep MI region at $V = 25E_r$, the oscillation amplitude $A$ characterizes multiple occupancies as the excitation for such non-steady states ramping across phase transition. Since this lack of thermalization and subsequent oscillation is the direct consequence of the gap-opening process, the scaling dependence $A \sim k^{3/2}$ provides a new relation in the non-steady-state region which is linked to the quantum phase transition but was not explored by conventional KZM.

Based on different observables, we get two different values for the same quantum critical parameter $\nu z$, namely, $\nu z = 1$ for the MI dynamical relaxation time $\tau_{\mathrm{MI}}$ and $\nu z = 1/2$ for the excitation fraction $n_{\mathrm{ex}}$. According to conventional KZM, the universality of the quantum criticality predicts the same value of $\nu z$ for different observables in the same QPT. Thus, our measurement results contradict the conventional KZM. According to previous studies [25,26], $\nu z$ is either 1 or $1/2$ depending on whether the phase transition point is off tip or on tip and how the gaps open in the SF-MI phase diagram [Fig. 4(d)]. Because of the harmonic trap and fixed atom number in our experiment, we probe the phase transition with an unfixed chemical potential, corresponding to a line, not a point in the phase diagram. The center filling of the final stage of MI is approximately $\bar{n} \sim 3$. In the scenario of a slow ramp, the MI appear and coexist with SF while the trap depth is not deep enough. Because the local gap opens as $\Delta \propto |g|^{1/2}$, the early-formed MI defects appear in the region of MI under the quantum criticality of $\nu z = 1/2$. Later when the trap depth increases, the total system enters the region of off-tip phase transitions where the gap $\Delta \propto |g|$ opens linearly with $\nu z = 1$. However, the previously generated defects are still protected by the energy gaps under $U(1)$ symmetries with $\nu z = 1/2$. This is how both $\nu z$ appear in the same QPT experiment. If the QPT is performed in the opposite direction from gapped phases to gapless phases as in the previous experiments [23,24], the gapless excitations due to broken symmetries will smear out early formed defects with later dynamics and makes the different values of the quantum critical parameter indistinguishable. For a fast ramp, the system is immediately frozen into deep Mott insulators with failed relaxations due to large energy gaps, where the actual dynamics versus the excitation fractions or the correlation length is still an unexplored regime for nonequilibrium physics and waits for further investigations.

In conclusion, we observe the many-body quantum phase transition from gapless symmetry-broken phases to gapped symmetry-conserved phases. As the ramping gets faster, the critical behaviors change from retarded relaxations to phase oscillations. Even within the steady-state-relaxation regime, two different values for one critical parameter $\nu z$ are observed. The gap opening provides and protects different critical-mechanism competitions in the dynamics of many-body phase transitions. We believe this

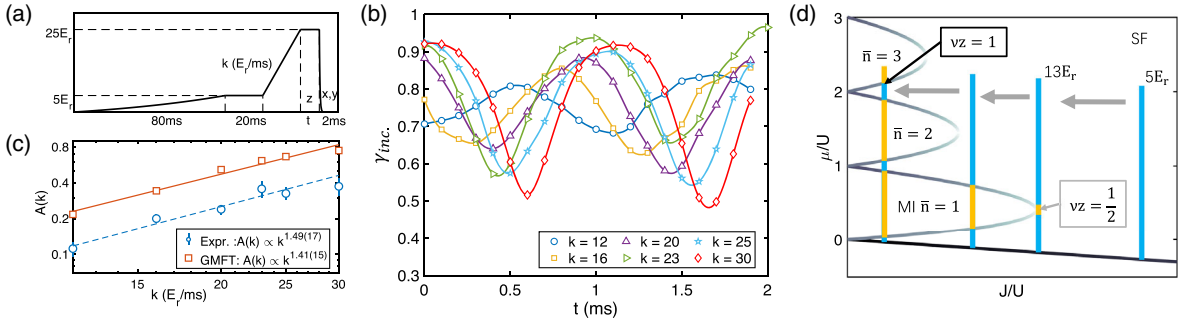


FIG. 4. Phase oscillations under a fast ramp. (a) Time sequences for oscillation measurements. The atoms are hold at $V = 25E_r$ for a varying time $t$. (b) $\gamma_{\mathrm{inc}}$ oscillates versus time $t$ for different $k$. The solid lines are cubic splines fit. (c) The fitted oscillation amplitude $A$ versus $k$. Blue circles are experimental data and the red squares are GMFT simulations. Two dashed lines are the fits based on power laws. For experimental data we obtain $A(k) \propto k^{1.49(17)}$, and the GMFT gives $A(k) \propto k^{1.41(15)}$. (d) An illustration of the dynamics in the SF-MI phase diagram. The blue lines represents our actual system and the on- or off-tip locations are labeled by arrows with $\nu z = 1/2$ or 1. The on-tip location has square-root gap opening and the off-tip one has linear gap opening.

inspires further investigations in the phase transition of symmetry-conserved gapped systems and the nonequilibrium physics.

We thank Hui Zhai, Joerg Schmiedmayer, Jakub Zakrzewski, and Bogdan Damski for helpful discussions. The numerical simulations are performed on High-Performance-Computing Platform of Peking University. This work is supported by the National Natural Science Foundation of China (Grants No. 91736208, No. 11974202, No. 61975092, No. 92165203, No. 11920101004, No. 61727819, No. 11934002) and the National Key Research and Development Program of China (Grant No. 2016YFA0301501).

[*]Present address: Department of Physics and Research Laboratory of Electronics, Massachusetts Institute of Technology, Cambridge, Massachusetts 02139, USA.
[†]cwlaser@ultracold.cn
[‡]xuzongchen@pku.edu.cn
[§]hujiazhong01@ultracold.cn

[1] F. Wilczek, Quantum Time Crystals, Phys. Rev. Lett. **109**, 160401 (2012).
[2] N. Goldman and J. Dalibard, Periodically Driven Quantum Systems: Effective Hamiltonians and Engineered Gauge Fields, Phys. Rev. X **4**, 031027 (2014).
[3] D. A. Abanin, E. Altman, I. Bloch, and M. Serbyn, Colloquium: Many-body localization, thermalization, and entanglement, Rev. Mod. Phys. **91**, 021001 (2019).
[4] R. Nandkishore and D. A. Huse, Many-body localization and thermalization in quantum statistical mechanics, Annu. Rev. Condens. Matter Phys. **6**, 15 (2015).
[5] P. C. Hendry, N. S. Lawson, R. A. M. Lee, P. V. E. McClintock, and C. D. H. Williams, Generation of defects in superfluid 4he as an analogue of the formation of cosmic strings, Nature (London) **368**, 315 (1994).
[6] C. Bäuerle, Yu. M. Bunkov, S. N. Fisher, H. Godfrin, and G. R. Pickett, Laboratory simulation of cosmic string formation in the early Universe using superfluid 3He, Nature (London) **382**, 332 (1996).
[7] N. Navon, A. L. Gaunt, R. P. Smith, and Z. Hadzibabic, Emergence of a turbulent cascade in a quantum gas, Nature (London) **539**, 72 (2016).
[8] S. Erne, R. Bücker, T. Gasenzer, J. Berges, and J. Schmiedmayer, Universal dynamics in an isolated one-dimensional Bose gas far from equilibrium, Nature (London) **563**, 225 (2018).
[9] M. Prüfer, P. Kunkel, H. Strobel, S. Lannig, D. Linnemann, C.-M. Schmied, J. Berges, T. Gasenzer, and M. K. Oberthaler, Observation of universal dynamics in a spinor Bose gas far from equilibrium, Nature (London) **563**, 217 (2018).
[10] T. W. B. Kibble, Topology of cosmic domains and strings, J. Phys. A **9**, 1387 (1976).
[11] W. H. Zurek, Cosmological experiments in superfluid helium?, Nature (London) **317**, 505 (1985).
[12] B. Ko, J. W. Park, and Y. Shin, Kibble–Zurek universality in a strongly interacting fermi superfluid, Nat. Phys. **15**, 1227 (2019).
[13] N. Navon, A. L. Gaunt, R. P. Smith, and Z. Hadzibabic, Critical dynamics of spontaneous symmetry breaking in a homogeneous Bose gas, Science **347**, 167 (2015).
[14] C. N. Weiler, T. W. Neely, D. R. Scherer, A. S. Bradley, M. J. Davis, and B. P. Anderson, Spontaneous vortices in the formation of Bose-Einstein condensates, Nature (London) **455**, 948 (2008).
[15] S. Ulm, J. Roßnagel, G. Jacob, C. Degünther, S. T. Dawkins, U. G. Poschinger, R. Nigmatullin, A. Retzker, M. B. Plenio, F. Schmidt-Kaler, and K. Singer, Observation of the Kibble-Zurek scaling law for defect formation in ion crystals, Nat. Commun. **4**, 2290 (2013).
[16] K. Pyka, J. Keller, H. L. Partner, R. Nigmatullin, T. Burgermeister, D. M. Meier, K. Kuhlmann, A. Retzker, M. B. Plenio, W. H. Zurek, A. del Campo, and T. E. Mehlstäubler, Topological defect formation and spontaneous symmetry breaking in ion coulomb crystals, Nat. Commun. **4**, 2291 (2013).
[17] P. Silvi, G. Morigi, T. Calarco, and S. Montangero, Crossover from Classical to Quantum Kibble-Zurek Scaling, Phys. Rev. Lett. **116**, 225701 (2016).
[18] L. W. Clark, L. Feng, and C. Chin, Universal space-time scaling symmetry in the dynamics of bosons across a quantum phase transition, Science **354**, 606 (2016).
[19] A. Keesling, A. Omran, H. Levine, H. Bernien, H. Pichler, S. Choi, R. Samajdar, S. Schwartz, P. Silvi, S. Sachdev, P. Zoller, M. Endres, M. Greiner, V. Vuletić, and M. D. Lukin, Quantum Kibble–Zurek mechanism and critical dynamics on a programmable Rydberg simulator, Nature (London) **568**, 207 (2019).
[20] M. Anquez, B. A. Robbins, H. M. Bharath, M. Boguslawski, T. M. Hoang, and M. S. Chapman, Quantum Kibble-Zurek Mechanism in a Spin-1 Bose-Einstein Condensate, Phys. Rev. Lett. **116**, 155301 (2016).
[21] L.-Y. Qiu, H.-Y. Liang, Y.-B. Yang, H.-X. Yang, T. Tian, Y. Xu, and L.-M. Duan, Observation of generalized Kibble-Zurek mechanism across a first-order quantum phase transition in a spinor condensate, Sci. Adv. **6**, eaba7292 (2020).
[22] X.-P. Liu, X.-C. Yao, Y. Deng, X.-Q. Wang, Y.-. Wang, C.-J. Huang, X. Li, Y.-A. Chen, and J.-W. Pan, Universal Dynamical Scaling of Quasi-Two-Dimensional Vortices in a Strongly Interacting Fermionic Superfluid, Phys. Rev. Lett. **126**, 185302 (2021).
[23] D. Chen, M. White, C. Borries, and B. DeMarco, Quantum Quench of an Atomic Mott Insulator, Phys. Rev. Lett. **106**, 235304 (2011).
[24] S. Braun, M. Friesdorf, S. S. Hodgman, M. Schreiber, J. P. Ronzheimer, A. Riera, M. del Rey, I. Bloch, J. Eisert, and U. Schneider, Emergence of coherence and the dynamics of quantum phase transitions, Proc. Natl. Acad. Sci. U.S.A. **112**, 3641 (2015).
[25] M. P. A. Fisher, P. B. Weichman, G. Grinstein, and D. S. Fisher, Boson localization and the superfluid-insulator transition, Phys. Rev. B **40**, 546 (1989).
[26] S. Sachdev, *Quantum Phase Transitions*, 2nd ed. (Cambridge University Press, Cambridge, England, 2011).
[27] D. Pekker, B. Wunsch, T. Kitagawa, E. Manousakis, A. S. Sørensen, and E. Demler, Signatures of the superfluid to Mott insulator transition in equilibrium and in dynamical ramps, Phys. Rev. B **86**, 144527 (2012).

[28] K. Shimizu, T. Hirano, J. Park, Y. Kuno, and I. Ichinose, Dynamics of first-order quantum phase transitions in extended Bose-Hubbard model: from density wave to superfluid and vice versa, New J. Phys. **20**, 083006 (2018).

[29] K. Shimizu, Y. Kuno, T. Hirano, and I. Ichinose, Dynamics of a quantum phase transition in the Bose-hubbard model: Kibble-Zurek mechanism and beyond, Phys. Rev. A **97**, 033626 (2018).

[30] A. Polkovnikov, Universal adiabatic dynamics in the vicinity of a quantum critical point, Phys. Rev. B **72**, 161201(R) (2005).

[31] A. Bermudez, D. Patanè, L. Amico, and M. A. Martin-Delgado, Topology-Induced Anomalous Defect Production by Crossing a Quantum Critical Point, Phys. Rev. Lett. **102**, 135702 (2009).

[32] A Bermudez, L Amico, and M. A. Martin-Delgado, Dynamical delocalization of majorana edge states by sweeping across a quantum critical point, New J. Phys. **12**, 055014 (2010).

[33] T. Zhou, R. Yao, K. Yang, S. Jin, Y. Zhai, X. Yue, S. Yang, X. Zhou, X. Chen, and X. Li, Dimension crossing turbulent cascade in an excited lattice bose gas, arXiv:1912.13252.

[34] T. Zhou, K. Yang, Y. Zhai, X. Yue, S. Yang, J. Xiang, Q. Huang, W. Xiong, X. Zhou, and X. Chen, High precision calibration of optical lattice depth based on multiple pulses Kapitza-Dirac diffraction, Opt. Express **26**, 16726 (2018).

[35] T. Luan, Y. Li, X. Zhang, and X. Chen, Realization of two-stage crossed beam cooling and the comparison with delta-kick cooling in experiment, Rev. Sci. Instrum. **89**, 123110 (2018).

[36] M. Greiner, O. Mandel, T. Esslinger, T. W. Hänsch, and I. Bloch, Quantum phase transition from a superfluid to a mott insulator in a gas of ultracold atoms, Nature (London) **415**, 39 (2002).

[37] See Supplemental Material at http://link.aps.org/supplemental/10.1103/PhysRevLett.127.200601 for more discussions and calculations.

[38] M. Köhl, H. Moritz, T. Stöferle, K. Günter, and T. Esslinger, Fermionic Atoms in a Three Dimensional Optical Lattice: Observing Fermi Surfaces, Dynamics, and Interactions, Phys. Rev. Lett. **94**, 080403 (2005).

[39] B. Capogrosso-Sansone, N. V. Prokof'ev, and B. V. Svistunov, Phase diagram and thermodynamics of the three-dimensional Bose-Hubbard model, Phys. Rev. B **75**, 134302 (2007).

[40] D. Jaksch, C. Bruder, J. I. Cirac, C. W. Gardiner, and P. Zoller, Cold Bosonic Atoms in Optical Lattices, Phys. Rev. Lett. **81**, 3108 (1998).

[41] J. Zakrzewski, Mean-field dynamics of the superfluid-insulator phase transition in a gas of ultracold atoms, Phys. Rev. A **71**, 043601 (2005).

[42] M. Greiner, O. Mandel, T. W. Hänsch, and I. Bloch, Collapse and revival of the matter wave field of a Bose-Einstein condensate, Nature (London) **419**, 51 (2002).